

NOTICE: this is the author's version of a work that was accepted for publication in International Journal of Hydrogen Energy. Changes resulting from the publishing process, such as peer review, editing, corrections, structural formatting, and other quality control mechanisms may not be reflected in this document. Changes may have been made to this work since it was submitted for publication. A definitive version was subsequently published in International Journal of Hydrogen Energy, Vol. 39, no. 28 (2014).

DOI: 10.1016/j.ijhydene.2014.03.077

**Performance stability and degradation mechanism of  $\text{La}_{0.6}\text{Sr}_{0.4}\text{Co}_{0.2}\text{Fe}_{0.8}\text{O}_{3-\delta}$  cathodes  
under solid oxide fuel cells operation conditions**

Yihui Liu<sup>a, b</sup>, Kongfa Chen<sup>b</sup>, Ling Zhao<sup>b</sup>, Bo Chi<sup>a, \*</sup>, Jian Pu<sup>a</sup>, San Ping Jiang<sup>b, \*</sup>, Li Jian<sup>a</sup>

<sup>a</sup> Center for Fuel Cell Innovation, School of Materials Science and Engineering, State Key Laboratory of Material Processing and Die & Mould Technology, Huazhong University of Science and Technology, Wuhan, Hubei 430074, PR China

<sup>b</sup> Fuels and Energy Technology Institute & Department of Chemical Engineering, Curtin University, Perth, WA 6102, Australia

**Abstract**

The performance stability and degradation mechanism of  $\text{La}_{0.6}\text{Sr}_{0.4}\text{Co}_{0.2}\text{Fe}_{0.8}\text{O}_{3-\delta}$  (LSCF) cathodes and LSCF impregnated  $\text{Gd}_{0.1}\text{Ce}_{0.9}\text{O}_{2-\delta}$  (LSCF-GDC) cathodes are investigated under solid oxide fuel cell operation conditions. LSCF and LSCF-GDC cathodes show initially performance improvement but degrade under cathodic polarization treatment at 750 °C for 120 h. The results confirm the grain growth and agglomeration of LSCF and in particular GDC-LSCF cathodes as well as the formation of  $\text{SrCoO}_x$  particles on the surface of LSCF under cathodic polarization conditions. The direct observation of  $\text{SrCoO}_x$  formation has been made possible on the surface of dense LSCF electrode plate on GDC electrolyte. The formation of  $\text{SrCoO}_x$  is most likely due to the interaction between the segregated Sr and Co from LSCF lattice under polarization conditions. The formation of  $\text{SrCoO}_x$  would contribute to the deterioration of the electrocatalytic activity of the LSCF-based electrodes for the  $\text{O}_2$

---

Email: [chibo@hust.edu.cn](mailto:chibo@hust.edu.cn) (Bo Chi), [s.jiang@curtin.edu.au](mailto:s.jiang@curtin.edu.au) (S.P. Jiang)  
Tel : +86 27 87558142(B. Chi), +61 8 9266 9804(S.P. Jiang)

reduction in addition to the agglomeration and microstructure coarsening.

**Keywords:** Solid oxide fuel cells; Stability; LSCF cathode; LSCF impregnated GDC; Current treatment; Degradation mechanism.

## 1. Introduction

Lanthanum strontium cobalt ferrite,  $\text{La}_{0.6}\text{Sr}_{0.4}\text{Co}_{0.2}\text{Fe}_{0.8}\text{O}_{3-\delta}$  (LSCF) is one of the most common cathodes used in the intermediate temperature solid oxide fuel cells (IT-SOFCs). It exhibits high catalytic activity as well as good ionic and electronic conductivities[1-7]. However, one of the major concerns for the practical application of LSCF cathodes is its performance instability[8-10]. Sr segregation on the surface of LSCF cathodes is generally considered to be responsible for the performance degradation under SOFC operation conditions[11-13]. In the case of LSCF composite cathodes prepared by impregnation or infiltration methods, grain growth and coarsening of LSCF nanoparticles is the most important reason for the reduced performance[14, 15]. LSCF cathodes also react with yttria-stabilized zirconia (YSZ) based electrolytes, leading to the formation of insulating  $\text{SrZrO}_3$  phase and thus degrading the cell performance[16, 17].

In addition to the effect of temperature on the particle agglomeration and segregation, the current polarization also plays an important role for the performance stability of SOFC electrodes[18, 19]. Hagen et al. reported that current polarization led to the local delamination between the (La, Sr) $\text{MnO}_3$  (LSM) cathode and YSZ electrolyte and the significant increase in the ohmic and polarization resistances[20]. On the other hand, we found that cathodic current polarization enhances the electrocatalytic activity of LSM electrodes for the  $\text{O}_2$  reduction

reaction and the most likely reason is due to the incorporation of strontium species originally segregated on the surface into the lattice of LSM under the cathodic polarization conditions[21, 22]. Most recently in situ X-ray photoelectron spectroscopy (XPS) study by Janek's group [23, 24] clearly showed the surface depletion of Sr under cathodic polarization and enrichment of Sr under anodic polarization conditions, consistent with the proposed activation and deactivation mechanism of the LSM cathodes[25]. However, the performance degradation mechanism of LSCF cathodes under the condition of current polarization is far from clear despite the importance of the LSCF cathode materials in SOFCs.

The present study focuses on the performance degradation mechanism of LSCF cathodes under typical SOFC operating conditions. The electrocatalytic activity, microstructure and phase stability of porous and dense LSCF cathodes, and LSCF impregnated GDC (LSCF-GDC) cathodes were studied at 750 °C in air under the current density of 200 and 500 mA cm<sup>-2</sup>. The purpose of using dense LSCF electrode is to facilitate the direct observation of microstructure changes and surface segregation characterizations. The results indicate that cathodic current polarization promotes the formation of SrCoO<sub>x</sub> phase and is detrimental to the stability of LSCF cathodes.

## **2. Experimental**

### ***2.1 Electrode preparation***

Gd-doped CeO<sub>2</sub> (GDC) electrolyte substrates were prepared from Gd<sub>0.1</sub>Ce<sub>0.9</sub>O<sub>2-δ</sub> (AGC Seimi Chemical Co. Ltd., Japan) powder by die pressing, followed by sintering at 1500 °C for 6 h. Thickness and diameter of the GDC pellets were 0.9 and 19 mm, respectively. La<sub>0.6</sub>Sr<sub>0.4</sub>Co<sub>0.2</sub>Fe<sub>0.8</sub>O<sub>3-δ</sub> (Fuel Cell Materials, USA) powder was mixed with ink vehicle (Fuel

Cell Materials, USA) in a weight ratio of 1:1 to form a slurry. The slurry was painted onto the dense GDC pellets and sintered at 1000 °C for 2 h.

LSCF-GDC composite cathode was prepared by impregnating LSCF into porous GDC scaffold on dense GDC electrolyte. GDC powder was mixed with ink vehicle in a weight ratio of 1:1 and then was painted onto the dense GDC pellets, followed by sintering at 1200 °C for 2 h to obtain a porous GDC scaffold with a thickness of ~10 μm and an area of 0.5 cm<sup>2</sup>. LSCF precursor with ionic concentration of 0.5 mol L<sup>-1</sup> was obtained by mixing La(NO<sub>3</sub>)<sub>3</sub>·6H<sub>2</sub>O, Sr(NO<sub>3</sub>)<sub>2</sub>, Co(NO<sub>3</sub>)<sub>2</sub>·6H<sub>2</sub>O and Fe(NO<sub>3</sub>)<sub>3</sub>·9H<sub>2</sub>O (99.9%, Sigma-Aldrich) at a molar ratio of La : Sr : Co : Fe = 6 : 4 : 2 : 8 in distilled water. The solution was then impregnated into the porous GDC scaffold at room temperature by using a micro-syringe, followed with oscillation by ultrasonic generator for 30 min. The infiltrated electrodes were calcinated at 800 °C in air for 1 h to form LSCF phase in the porous GDC electrode structure. LSCF loading was measured by weighting the electrodes before and after the impregnation treatment. The high loading was achieved by repeating the impregnation and calcination processes. Final LSCF loading of LSCF-GDC composite cathode was ~1.2 mgcm<sup>-2</sup>.

In order to study the effect of polarization on the surface segregation, dense LSCF pellets were used instead of porous LSCF electrodes. Dense LSCF pellets were prepared by die pressing LSCF powder, followed by sintering at 1350 °C for 5 h. The LSCF pellets were 0.3 mm in thickness and 10 mm in diameter. Dense LSCF pellets were then directly mounted on the surface of GDC electrolyte as SOFC cathodes with Pt counter electrode on the other side of the electrolyte to form the three-electrode configuration[26] for electrochemical measurement.

## ***2.2 Characterization***

Pt paste was painted on the opposite side of the electrolyte disc and baked at 900 °C in air for 2 h, to achieve the circular-shaped counter electrode and the ring-shaped reference electrode. Pt paste was also painted on the top of impregnated LSCF-GDC cathodes as the current collector. Pt mesh and Pt wire were used as the current collector and current probes for the measurement.

Polarization treatment was carried out at the current density of 200 and 500 mA cm<sup>-2</sup>. Electrochemical measurements were carried out at 750 °C in air under the condition of open circuit using a Gamry Reference 3000 Potentiostat. Impedance data were recorded in the frequency range from 0.1 Hz to 100 KHz with signal amplitude of 10 mV. The electrode polarization resistance ( $R_p$ ) was measured by the differences between the high and low frequency intersections of the impedance spectrum in the first quadrant on the real axis ( $Z_{real}$  axis), and the ohmic resistance ( $R_o$ ) was obtained from the value of the high frequency intercept.

X-ray diffractometer (XRD, Bruker D8 Advance Diffractometer) with Cu K $\alpha$  radiation was adopted to identify the phase composition of as-prepared and post-test cells within the  $2\theta$  angle of 20-80° at room temperature. Scanning electron microscopy (SEM, NEON 40EsB) was used to examine the microstructure characterization. X-ray photoelectron spectroscopy (XPS, VG Multilab 2000) was employed to study the surface chemistry of cathodes.

## **3. Results and discussion**

### ***3.1 Electrochemical performance of LSCF cathodes***

Fig. 1 is the electrochemical impedance spectra of LSCF cathodes following polarization at  $200 \text{ mA cm}^{-2}$  and  $750 \text{ }^\circ\text{C}$  in air. The impedance curves were measured under open circuit as a function of polarization time. The initial  $R_p$  is  $0.19 \text{ } \Omega \text{ cm}^2$  and increases to  $0.62 \text{ } \Omega \text{ cm}^2$  after polarized at  $200 \text{ mA cm}^{-2}$  for 120 h. The electrode ohmic resistance  $R_o$  decreases slightly from  $3.86$  to  $3.68 \text{ } \Omega \text{ cm}^2$  in the first 2 h polarization and then increases to  $4.24 \text{ } \Omega \text{ cm}^2$  at the end of the polarization treatment. The overpotential,  $\eta$  shows a rapid increase initially, followed by a gradual increase with the polarization time (Fig.1b). This shows that the electrocatalytic activity of LSCF electrodes for the  $\text{O}_2$  reduction reaction degrades under cathodic polarization at  $200 \text{ mA cm}^{-2}$ , indicated by the continuous increase of  $R_p$ ,  $R_o$  and  $\eta$ .

The impedance response for the  $\text{O}_2$  reduction on the LSCF electrodes at  $750 \text{ }^\circ\text{C}$  is characterized by two separated impedance arcs at low and high frequencies in the initial stage of polarization. After polarized at  $200 \text{ mA cm}^{-2}$  for 48 h, the low and high frequency arcs overlap, forming a depressed and large impedance arc (Fig. 1a). The electrochemical impedance responses were fitted with an equivalent circuit of  $R_o(Q_1 R_{p,H})(Q_2 R_{p,L})$ , where  $R_o$  is the electrode ohmic resistance,  $Q_1$  and  $Q_2$  are the constant phase elements,  $R_{p,H}$  and  $R_{p,L}$  are the electrode polarization resistance of high and low frequencies.  $R_{p,H}$  represents the charge transfer (electron and oxygen ion transfer) process, whereas  $R_{p,L}$  represents the mass transfer (oxygen adsorption, dissociation and diffusion) process[27]. The dependence of  $R_p$ ,  $R_{p,H}$  and  $R_{p,L}$  on the polarization time is shown in Fig. 1c.  $R_{p,H}$  shows relatively minor variation with polarization time and the increase of  $R_p$  is mainly contributed by the increase of  $R_{p,L}$ . This indicates that the polarization losses for the  $\text{O}_2$  reduction reaction on LSCF under a cathodic current of  $200 \text{ mA cm}^{-2}$  are mainly related to the low frequency electrode process associated

with the oxygen adsorption, dissociation and diffusion.

Fig. 2 shows the electrochemical impedance spectra of LSCF cathodes as a function of polarization time at 500 mA cm<sup>-2</sup> and 750 °C in air.  $R_o$  decreases significantly from 5.03 to 2.02  $\Omega$  cm<sup>2</sup> after polarized for 120 h, indicating that high current improves the electrical contact between the LSCF electrode and GDC electrolyte.  $R_p$  also decreases from 0.87 to 0.17  $\Omega$  cm<sup>2</sup> in the first 8 h treatment and increases again to 0.45  $\Omega$  cm<sup>2</sup> after 120 h treatment. The change of the  $R_p$  as a function of polarization at a high current of 500 mA cm<sup>-2</sup> indicates the complicated effect of the polarization on the performance stability of LSCF electrodes (Fig. 2c). The initial polarization behavior of LSCF under 500 mA cm<sup>-2</sup> is similar to that observed under a lower current of 200 mA cm<sup>-2</sup> (Fig. 2b). However, after polarized for 16 h,  $\eta$  essentially remains constant with further polarization at 500 mA cm<sup>-2</sup> though it is fluctuated significantly during the polarization period.

### ***3.2 Electrochemical performance of impregnated LSCF-GDC cathodes***

Fig. 3 shows the electrochemical impedance spectra and the variation of  $R_o$  and  $R_p$  of the impregnated LSCF-GDC cathodes measured at 200 mA cm<sup>-2</sup> and 750 °C in air.  $R_o$  decreases rapidly from 3.43 to 2.74  $\Omega$  cm<sup>2</sup> after 2 h treatment and remains more or less stable. In case of  $R_p$ , it decreases rapidly from 1.4 to 0.18  $\Omega$  cm<sup>2</sup> after 2 h treatment, followed by a very slow increase with the polarization time (Fig. 3b). After polarized for 120 h,  $R_p$  is 0.34  $\Omega$  cm<sup>2</sup>, still significantly lower than the initial  $R_p$  of 1.4  $\Omega$  cm<sup>2</sup>. This indicates that effect of the polarization at 200 mA cm<sup>-2</sup> on the electrocatalytic activity of nano-structured LSCF-GDC composite electrodes is quite small.

The electrochemical impedance behavior of the LSCF-GDC composite cathodes were

also measured at  $500 \text{ mA cm}^{-2}$  and  $750 \text{ }^\circ\text{C}$  in air and the results are shown in Fig. 4.  $R_o$  decreases from  $3.86$  to  $2.87 \text{ } \Omega \text{ cm}^2$  in the first 4 h polarization and increases again to  $3.6 \text{ } \Omega \text{ cm}^2$  after polarization for 120 h. On the other hand,  $R_p$  shows a significant increase with the polarization at  $500 \text{ mA cm}^{-2}$ , reaching  $2.15 \text{ } \Omega \text{ cm}^2$  after 120 h treatment, two times higher as compared to the initial  $R_p$  value,  $0.68 \text{ } \Omega \text{ cm}^2$ . Different from the electrode behavior polarized at  $200 \text{ mA cm}^{-2}$ , polarization at a high current of  $500 \text{ mA cm}^{-2}$  accelerates and causes serious performance degradation of LSCF-GDC cathodes.

### 3.3 Microstructure

Fig.5 is the SEM micrographs of LSCF cathodes before and after current treatment. As-prepared LSCF cathodes show uniform porous structure and the average size of LSCF particles is  $143 \pm 29 \text{ nm}$  (Fig. 5a). Under the condition of open circuit at  $750 \text{ }^\circ\text{C}$  for 120 h, LSCF particles grow to  $\sim 205 \pm 40 \text{ nm}$  (Fig. 5b). After polarization treatment at  $200 \text{ mA cm}^{-2}$  and  $750 \text{ }^\circ\text{C}$  for 120 h, the size of LSCF particles is  $222 \pm 58 \text{ nm}$  (Fig. 5c). When the current treatment increased to  $500 \text{ mA cm}^{-2}$ , the agglomeration seems more significant and the average size of LSCF particles increases to  $235 \pm 38 \text{ nm}$  (Fig. 5d).

Fig. 6 shows SEM micrographs of cross-sections of impregnated LSCF-GDC cathodes. Before the treatment, the as-prepared cathodes are characterized by fine LSCF particles with the average size of  $22 \pm 4 \text{ nm}$  dispersing on the porous GDC scaffold (Fig. 6a). Under open circuit condition at  $750 \text{ }^\circ\text{C}$  for 120 h, few change of cathode microstructure is observed and the average size of LSCF particles is  $21 \pm 3 \text{ nm}$  (Fig. 6b). After current polarization at  $200 \text{ mA cm}^{-2}$  and  $750 \text{ }^\circ\text{C}$  for 120 h, the size of impregnated LSCF nanoparticles is  $26 \pm 4 \text{ nm}$  (Fig. 6c). However, the LSCF particles on the surface of GDC scaffold appear to be flattened (shown as

insert in Fig. 6c). The flattening of impregnated nanoparticles has also been observed in nano-structured LSCF-YSZ cathodes[28] and nano-structured  $\text{La}_{0.8}\text{Sr}_{0.2}\text{FeO}_3$ -YSZ cathodes[29]. This indicates that nano-sized particles have the tendency to reduce their high surface areas under the SOFC operation conditions. The microstructure of LSCF-GDC electrodes after the polarization treatment under a high current of  $500 \text{ mA cm}^{-2}$  is very different from that after a low current polarization treatment. Impregnated LSCF nanoparticles agglomerates together, forming larger strip-shaped particles with a significantly reduced porosity after current polarization at  $500 \text{ mA cm}^{-2}$  for 120 h (shown as insert in Fig. 6d). The significant agglomeration and formation of large strip-type particles would lead to the reduced surface areas of the LSCF-GDC electrodes, consistent with the significant increase in  $R_o$  and  $R_p$ , as shown in Fig. 4.

### ***3.4 Dense LSCF cathodes***

In order to better observe the morphological change on the surface of LSCF electrode under the influence of cathodic polarization conditions, dense LSCF electrodes were prepared on top of GDC electrolyte pellets, followed by polarization treatment similar to that on the porous LSCF electrodes. Fig. 7 is the SEM micrographs of dense LSCF electrodes before and after polarization current treatment. The surface of as-prepared dense LSCF is smooth with clear grain boundaries (Fig. 7a). After treatment at  $750 \text{ }^\circ\text{C}$  for 120 h under open circuit, few fine particles appear on the surface (Fig. 7b). Significant change occurs for the samples after current treatment at  $200 \text{ mA cm}^{-2}$  for 24 h. Large numbers of particles with the average size of  $70 \pm 15 \text{ nm}$  were formed on the surface of dense LSCF, indicating that current treatment leads to the segregation and formation of these fine particles (Fig. 7c). When the polarization

period increased to 120 h, there seems to be reduction in fine particles and strip-shaped particles with the length of  $430\pm 98$  nm were observed on the surface of LSCF grain and particles as large as  $227\pm 20$  nm on the grain boundaries (Fig. 7d). The formation and agglomeration of fine particles on the LSCF surface indicates the surface segregation on the LSCF, consistent with those reported in the literature[11-13].

Fig. 8 is the XRD patterns of dense LSCF cathodes before and after polarization treatment at 750 °C in air for 120 h under different current densities. As-prepared LSCF sample shows only typical perovskite peaks (curve a in Fig.8). And after testing at 750 °C in air under open circuit for 120 h, there is basically no change in the XRD patterns (curve b in Fig.8). However, after testing at 750 °C and  $100 \text{ mA cm}^{-2}$  in air for 120 h, the majority of phases are still LSCF perovskite. Increasing the polarization current to  $200 \text{ mA cm}^{-2}$  for 120 h, a peak at  $2\theta$  around  $29^\circ$  suggests the formation of a second phase,  $\text{SrCoO}_x$  [30] (shown as insert in Fig. 8). This indicates that cathodic current polarization causes the formation of  $\text{SrCoO}_x$  phase on the LSCF surface. Thus, the strip-shaped particles observed on LSCF (Fig.7c and d) are most likely the  $\text{SrCoO}_x$  phase formed under cathodic polarization conditions.

XPS was employed to study the surface chemistry of the dense LSCF electrodes before and after the polarization treatment, as shown in Fig. 9. Relative atomic concentrations were calculated by the peak area of element XPS spectra. Binding energies and relative atomic concentrations are summarized in Table 1. Two states have been observed in XPS spectra of O 1s in LSCF; surface state are responsible for the XPS peak at 531-532 eV while bulk-bound states are responsible for the peak at 528.5 eV[31]. The changes in the XPS peak

for the O 1s are very small. However, the XPS peak at 528.5 eV decreases in intensity after treatment under open circuit or under the current density of 200 and 500 mA cm<sup>-2</sup>. This indicates that bulk-bound oxygen species decrease due to the treatment, suggesting oxides other than LSCF may have formed on the surface of LSCF under open circuit and current polarization conditions.

In case of La, the binding energy for the La 3d<sub>5/2</sub> peak of LSCF before treatment is 832.97 eV. After treatment at 750 °C under open circuit, the binding energy is 832.58 eV. After polarization treatment under the current density of 200 and 500 mA cm<sup>-2</sup>, the binding energy is 833.45 and 832.71 eV, respectively. These four values of binding energies all agree well with La<sup>3+</sup> compounds[31], indicating no obvious change in valence state under the polarization treatment. Similarly, the binding energy for the Fe 2p<sub>3/2</sub> peak of LSCF under the above-mentioned conditions is 709.21, 709.1, 709.4 and 709.37 eV, respectively, which agrees well with the values of Fe in LSCF[32].

In case of Sr, the binding energy for the Sr 3d<sub>5/2</sub> peak of LSCF before treatment is 131.78 eV. After treatment at 750 °C for 120 h under open circuit, the binding energy is 131.66 eV, very close to that of as-prepared LSCF sample. And after polarization treatment for 120 h under the current density of 100 mA cm<sup>-2</sup>, the binding energy is 131.54 eV. The difference between these values is within the accepted measurement limits of XPS technique. Hence, all of them correspond to bulk-bound state Sr[31], indicating that open circuit and current treatment at 100 mA cm<sup>-2</sup> have little effect on the valence state of Sr. However, the binding energy for the Sr 3d<sub>5/2</sub> peak increases to 132.45 eV after current treatment at 200 mA cm<sup>-2</sup> for 120 h, indicating the existence of surface state Sr.

Significant changes of the binding energies for the Co 2p spectrum were also observed. The binding energy for the Co 2p<sub>3/2</sub> peak of LSCF before and after treatment at 750 °C under open circuit for 120 h is 779.57 and 779.56 eV, indicating no obvious changes in the state of cobalt. However, the binding energy of Co 2p<sub>3/2</sub> for LSCF after current treatment at 100 and 200 mA cm<sup>-2</sup> and 750 °C for 120 h is 778.99 and 779.06 eV, respectively. The decrease of binding energy suggests the valence change of Co<sup>2+</sup> to Co<sup>3+</sup> [32].

As shown in Table 1, the La/Sr ratio in the as-prepared LSCF and LSCF after heat treatment at 750°C for 120 h is 0.55 and 0.61, which is much smaller than the stoichiometric La/Sr ratio of 1.5 in LSCF, suggesting that Sr segregation causes the Sr enrichment on the surface of LSCF. However, after treatment at 750 °C for 120 h at 100 and 200 mA cm<sup>-2</sup>, the La/Sr ratio increases to 1.36 and 0.76, respectively. The decrease of Sr concentration on the surface implies the incorporation of Sr into the lattice of LSCF under polarization conditions [23-25]. The La/Sr ratio after current polarization is still smaller than the stoichiometric ratio of 1.5 for LSCF, indicating Sr segregation or enrichment still exist on the surface of LSCF under SOFC operation conditions. The atomic concentration of Co on the surface of LSCF after current treatment at 100 and 200 mA cm<sup>-2</sup> increases obviously, which can be contributed to the Co migration to the surface caused by current polarization. The result is consistent with the previous study, showing that Co segregation on the surface of LSCF after operation[33].

The electrochemical performance results in the present study show that cathodic polarization at 200 mA cm<sup>-2</sup> causes the performance degradation of LSCF cathodes for the O<sub>2</sub> reduction reaction and increase in the current density accelerates the degradation process. As shown by the XPS results, cathodic current treatment may facilitate the formation of SrCoO<sub>x</sub>

phases due to the segregation of Sr and Co species on the LSCF surface, though cathodic polarization could lead to the incorporation of Sr into the lattice of LSCF. The significant formation of  $\text{SrCoO}_x$  phase on the surface of LSCF-based electrodes under polarization conditions can cause the degradation of the electrocatalytic activity of the electrodes, in addition to the agglomeration and growth of LSCF and impregnated LSCF nanoparticles.

## 5. Conclusions

The stability of LSCF cathodes and impregnated LSCF-GDC cathodes was investigated under polarization current of 200 and 500  $\text{mA cm}^{-2}$  at 750°C. The performance of both LSCF and impregnated LSCF-GDC cathodes in general shows degradation under cathodic current treatment, particularly under high polarization current densities. Polarization at high current density of 500  $\text{mA cm}^{-2}$  significantly accelerates the performance degradation. SEM results indicate the agglomeration and microstructure deterioration of the LSCF and LSCF-GDC composite electrodes. On dense LSCF cathode samples, XRD and SEM results show clearly that cathodic current treatment results in the formation of  $\text{SrCoO}_x$  particles on the electrode surface. The formation of secondly phase,  $\text{SrCoO}_x$ , is considered to contribute significantly to the degradation of the electrochemical activity of the LSCF based electrode for the  $\text{O}_2$  reduction reaction, in addition to the performance degradation caused by the agglomeration and coarsening of the LSCF and LSCF-GDC electrodes.

## Acknowledgements

This work was financially supported by the Australian Research Council (LP110200281), the National Natural Science foundation of China (U1134001) and the National “863” project

of China (2011AA050702). XRD and SEM examinations were assisted by the Curtin X-Ray Laboratory and Curtin University Electron Microscopy Facility, both of which are partially funded by the University, State and Commonwealth Governments.

## References

- [1] Jiang SP. A comparison of O<sub>2</sub> reduction reactions on porous (La,Sr)MnO<sub>3</sub> and (La,Sr)(Co,Fe)O<sub>3</sub> electrodes. *Solid State Ionics* 2002; 146:1-22.
- [2] Tai LW, Nasrallah MM, Anderson HU, Sparlin DM, Sehlin SR. Structure and electrical properties of La<sub>1-x</sub>Sr<sub>x</sub>Co<sub>1-y</sub>Fe<sub>y</sub>O<sub>3</sub>. Part 2. The system La<sub>1-x</sub>Sr<sub>x</sub>Co<sub>0.2</sub>Fe<sub>0.8</sub>O<sub>3</sub>. *Solid State Ionics* 1995; 76:273-83.
- [3] Mai A, Haanappel VAC, Uhlenbruck S, Tietz F, Stover D. Ferrite-based perovskites as cathode materials for anode-supported solid oxide fuel cells Part I. Variation of composition. *Solid State Ionics* 2005; 176:1341-50.
- [4] Esquirol A, Brandon NP, Kilner JA, Mogensen M. Electrochemical characterization of La<sub>0.6</sub>Sr<sub>0.4</sub>Co<sub>0.2</sub>Fe<sub>0.8</sub>O<sub>3</sub> cathodes for intermediate-temperature SOFCs. *J Electrochem Soc* 2004; 151:A1847-A55.
- [5] Marinha D, Dessemond L, Cronin JS, Wilson JR, Barnett SA, Djurado E. Microstructural 3D reconstruction and performance evaluation of LSCF cathodes obtained by electrostatic spray deposition. *Chem Mat* 2011; 23:5340-8.
- [6] Steele BCH, Bae JM. Properties of La<sub>0.6</sub>Sr<sub>0.4</sub>Co<sub>0.2</sub>Fe<sub>0.8</sub>O<sub>3-x</sub> (LSCF) double layer cathodes on gadolinium-doped cerium oxide (CGO) electrolytes - II. Role of oxygen exchange and diffusion. *Solid State Ionics* 1998; 106:255-61.
- [7] Grunbaum N, Dessemond L, Fouletier J, Prado F, Mogni L, Caneiro A. Rate limiting steps of the porous La<sub>0.6</sub>Sr<sub>0.4</sub>Co<sub>0.8</sub>Fe<sub>0.2</sub>O<sub>3-δ</sub> electrode material. *Solid State Ionics* 2009; 180:1448-52.
- [8] Yokokawa H, Tu H, Iwanschitz B, Mai A. Fundamental mechanisms limiting solid oxide fuel cell durability. *J Power Sources* 2008; 182:400-12.
- [9] Lee S, Miller N, Gerdes K. Long-term stability of SOFC composite cathode activated by electrocatalyst infiltration. *J Electrochem Soc* 2012; 159:F301-8.
- [10] Tietz F, Haanappel VAC, Mai A, Mertens J, Stover D. Performance of LSCF cathodes in cell tests. *J Power Sources* 2006; 156:20-2.
- [11] Oh MY, Unemoto A, Amezawa K, Kawada T. Stability of La<sub>0.6</sub>Sr<sub>0.4</sub>Co<sub>0.2</sub>Fe<sub>0.8</sub>O<sub>3-δ</sub> as SOFC cathode. *J Electrochem Soc* 2012; 159:F659-64.
- [12] Simner SP, Anderson MD, Engelhard MH, Stevenson JW. Degradation mechanisms of La-Sr-Co-Fe-O<sub>3</sub> SOFC cathodes. *Electrochem Solid State Lett* 2006; 9:A478-A81.
- [13] Oh D, Gostovic D, Wachsman ED. Mechanism of La<sub>0.6</sub>Sr<sub>0.4</sub>Co<sub>0.2</sub>Fe<sub>0.8</sub>O<sub>3</sub> cathode degradation. *J Mater Res* 2012; 27:1992-9.
- [14] Shah M, Voorhees PW, Barnett SA. Time-dependent performance changes in LSCF-infiltrated SOFC cathodes: The role of nano-particle coarsening. *Solid State Ionics* 2011; 187:64-7.
- [15] Liu Y, Chen J, Wang F, Chi B, Pu J, Li J. Performance stability of impregnated La<sub>0.6</sub>Sr<sub>0.4</sub>Co<sub>0.2</sub>Fe<sub>0.8</sub>O<sub>3-δ</sub>-Y<sub>2</sub>O<sub>3</sub> stabilized ZrO<sub>2</sub> cathodes of intermediate temperature solid oxide fuel cells. *Int J Hydrog Energy*

- 2014; 39:3404-11.
- [16] Mai A, Becker M, Assenmacher W, Tietz F, Hathiramani D, Ivers-Tiffée E, Stover D, Mader W. Time-dependent performance of mixed-conducting SOFC cathodes. *Solid State Ionics* 2006; 177:1965-8.
- [17] Pena-Martinez J, Marrero-Lopez D, Sanchez-Bautista C, Dos Santos-Garcia AJ, Ruiz-Morales JC, Canales-Vazquez J, Nunez P. Effect of a CGO buffer layer on the performance of  $(\text{La}_{0.6}\text{Sr}_{0.4})_{0.995}\text{Co}_{0.2}\text{Fe}_{0.8}\text{O}_{3-\delta}$  cathode in YSZ-Based SOFC. *Bol Soc Esp Ceram Vidr* 2010; 49:15-22.
- [18] Jiang SP, Love JG. Observation of structural change induced by cathodic polarization on  $(\text{La,Sr})\text{MnO}_3$  electrodes of solid oxide fuel cells. *Solid State Ionics* 2003; 158:45-53.
- [19] Jiang SP, Wang W. Effect of polarization on the interface between  $(\text{La,Sr})\text{MnO}_3$  electrode and  $\text{Y}_2\text{O}_3\text{-ZrO}_2$  electrolyte. *Electrochem Solid State Lett* 2005; 8:A115-8.
- [20] Hagen A, Barfod R, Hendriksen PV, Liu YL, Ramousse S. Degradation of anode supported SOFCs as a function of temperature and current load. *J Electrochem Soc* 2006; 153:A1165-71.
- [21] Jiang SP. Activation, microstructure, and polarization of solid oxide fuel cell cathodes. *J Solid State Electrochem* 2007; 11:93-102.
- [22] Wang W, Jiang SP. Effect of polarization on the electrode behavior and microstructure of  $(\text{La,Sr})\text{MnO}_3$  electrodes of solid oxide fuel cells. *J Solid State Electrochem* 2004; 8:914-22.
- [23] Huber A-K, Falk M, Rohnke M, Luerssen B, Amati M, Gregoratti L, Hesse D, Janek J. In situ study of activation and de-activation of LSM fuel cell cathodes – Electrochemistry and surface analysis of thin-film electrodes. *Journal of Catalysis* 2012; 294:79-88.
- [24] Huber A-K, Falk M, Rohnke M, Luer, Gregoratti L, Amati M, Janek J. In situ study of electrochemical activation and surface segregation of the SOFC electrode material  $\text{La}_{0.75}\text{Sr}_{0.25}\text{Cr}_{0.5}\text{Mn}_{0.5}\text{O}_{3\pm\delta}$ . *Phys Chem Chem Phys* 2012; 14:751-8.
- [25] Wang W, Jiang SP. A mechanistic study on the activation process of  $(\text{La, Sr})\text{MnO}_3$  electrodes of solid oxide fuel cells. *Solid State Ionics* 2006; 177:1361-9.
- [26] Winkler J, Hendriksen PV, Bonanos N, Mogensen M. Geometric requirements of solid electrolyte cells with a reference electrode. *J Electrochem Soc* 1998; 145:1184-92.
- [27] Liang FL, Chen J, Chi B, Pu J, Jiang SP, Li J. Redox behavior of supported Pd particles and its effect on oxygen reduction reaction in intermediate temperature solid oxide fuel cells. *J Power Sources* 2011; 196:153-8.
- [28] Liu Y, Chi B, Pu J, Li J. Performance degradation of impregnated  $\text{La}_{0.6}\text{Sr}_{0.4}\text{Co}_{0.2}\text{Fe}_{0.8}\text{O}_3+\text{Y}_2\text{O}_3$  stabilized  $\text{ZrO}_2$  composite cathodes of intermediate temperature solid oxide fuel cells. *Int J Hydrog Energy* 2012; 37:4388-93.
- [29] Wang WS, Gross MD, Vohs JM, Gorte RJ. The stability of LSF-YSZ electrodes prepared by infiltration. *J Electrochem Soc* 2007; 154:B439-45.
- [30] Tolochko SP, Kononyuk IF, Ivashkevich LS, Lyakhov AS. Phase-composition and electrical-properties of  $\text{Bi}_{1-x}\text{Sr}_x\text{CoO}_y$  ( $X=0.1-1.0$ ). *Inorg Mater* 1993; 29:1375-9.
- [31] van der Heide PAW. Systematic x-ray photoelectron spectroscopic study of  $\text{La}_{1-x}\text{Sr}_x$ -based perovskite-type oxides. *Surface and Interface Analysis* 2002; 33:414-25.
- [32] Choudhury T, Saied SO, Sullivan JL, Abbot AM. Reduction of oxides of iron, cobalt, titanium and niobium by low-energy ion bombardment. *Journal of Physics D: Applied Physics* 1989; 22:1185-95.
- [33] Liu MF, Ding D, Blinn K, Li XX, Nie LF, Liu M. Enhanced performance of LSCF cathode through surface modification. *Int J Hydrog Energy* 2012; 37:8613-20.

## Figure captions

1. (a) Electrochemical impedance spectra, (b) polarization curves and (c) plots of  $R_o$ ,  $R_p$ ,  $R_{p,H}$  and  $R_{p,L}$  of LSCF cathodes as a function of polarization time, measured at 200 mA cm<sup>-2</sup> and 750 °C in air.
2. (a) Electrochemical impedance spectra, (b) polarization curves and (c) plots of  $R_o$ ,  $R_p$ , of LSCF cathodes as a function of polarization time, measured at 500 mA cm<sup>-2</sup> and 750 °C in air.
3. (a) Electrochemical impedance spectra, and (b) plots of  $R_o$ ,  $R_p$ , of impregnated LSCF-GDC cathodes as a function of polarization time, measured at 200 mA cm<sup>-2</sup> and 750 °C in air.
4. (a) Electrochemical impedance spectra, and (b) plots of  $R_o$ ,  $R_p$ , of impregnated LSCF-GDC cathodes as a function of polarization time, measured at 500 mA cm<sup>-2</sup> and 750 °C in air.
5. SEM micrographs of fractured cross-sections of LSCF cathodes (a) as prepared, (b) under open circuit at 750 °C in air for 120 h, (c) polarized at 200 mA cm<sup>-2</sup> and 750°C for 120 h, and (d) polarized at 500 mA cm<sup>-2</sup> and 750°C for 120 h.
6. SEM micrographs of fractured cross-sections of impregnated LSCF-GDC cathodes (a) as prepared, (b) under open circuit at 750 °C in air for 120 h, (c) polarized at 200 mA cm<sup>-2</sup> and 750°C for 120 h, and (d) polarized at 500 mA cm<sup>-2</sup> and 750°C for 120 h.
7. SEM micrographs of the surface of dense LSCF (a) as prepared, (b) under open circuit at 750 °C in air for 120 h, (c) polarized at 200 mA cm<sup>-2</sup> and 750 °C for 24 h, and (d) polarized at 200 mA cm<sup>-2</sup> and 750 °C for 120 h.

8. XRD patterns of dense LSCF cathodes: (a) as-prepared, (b) under open circuit at 750 °C in air for 120 h, (c) polarized at 100 mA cm<sup>-2</sup> and 750 °C for 120 h, and (d) polarized at 200 mA cm<sup>-2</sup> and 750 °C for 120 h. The insert is magnified XRD patterns for  $29^\circ \leq 2\theta \leq 30^\circ$ .
9. The XPS spectra of the survey and O 1s, La 3d, Sr 3d, Co 2p, Fe 2p peaks of dense LSCF cathodes; (a) as-prepared, (b) under open circuit at 750 °C in air for 120 h, (c) polarized at 100 mA cm<sup>-2</sup> and 750 °C for 120 h, and (d) polarized at 200 mA cm<sup>-2</sup> and 750°C for 120 h.

**Table 1.**

Binding energies and relative atomic concentrations determined by XPS for dense LSCF cathodes before and after polarization treatment at 750 °C in air for 120 h under different current densities.

Element	As-prepared		open circuit		100 mA cm <sup>-2</sup>		200 mA cm <sup>-2</sup>	
	Binding energy(eV)	at.%	Binding energy(eV)	at.%	Binding energy(eV)	at.%	Binding energy(eV)	at.%
O 1s	531.33	—	531.56	—	531.24	—	531.41	—
La 3d5/2	832.97	27.22	832.58	25.73	833.45	38.28	832.71	27.73
Sr 3d5/2	131.78	41.18	131.66	42.4	131.54	28.19	132.45	36.59
Co 2p3/2	779.57	8.69	779.56	6.91	778.99	9.03	779.06	9.93
Fe 2p3/2	709.21	22.91	709.1	24.96	709.4	24.5	709.37	25.75
La/Sr	—	0.55	—	0.61	—	1.36	—	0.76

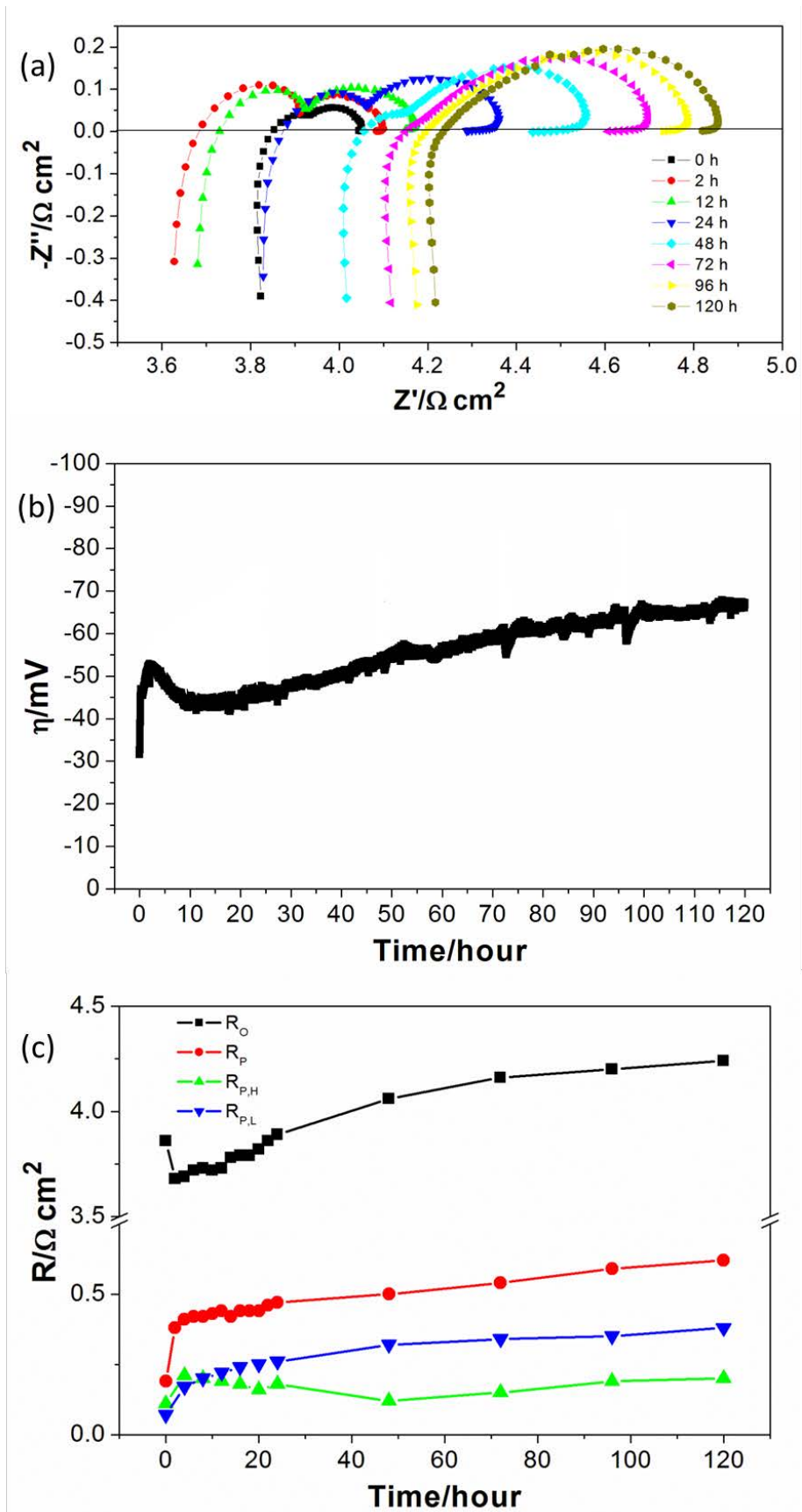


Fig. 1

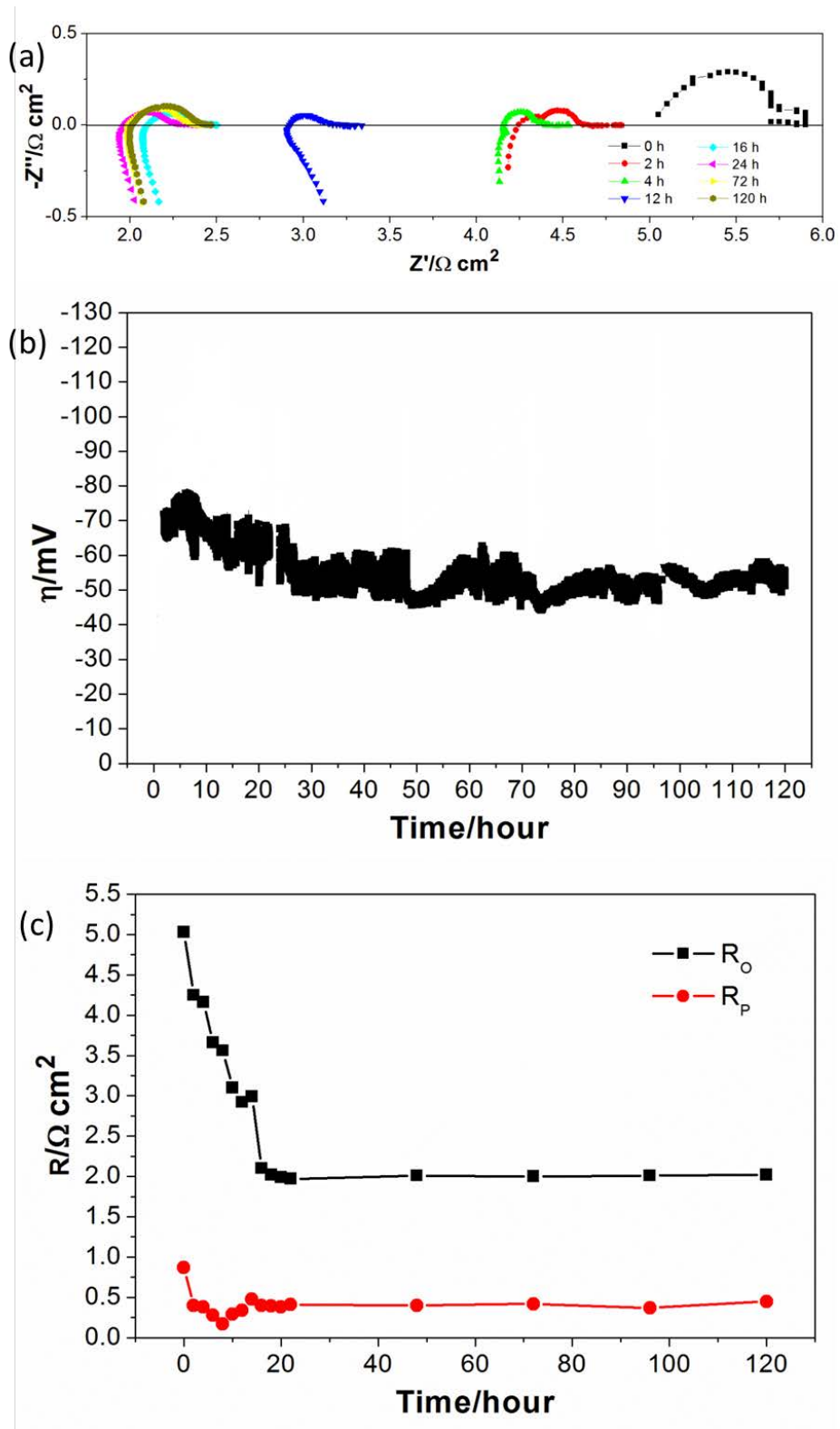


Fig. 2

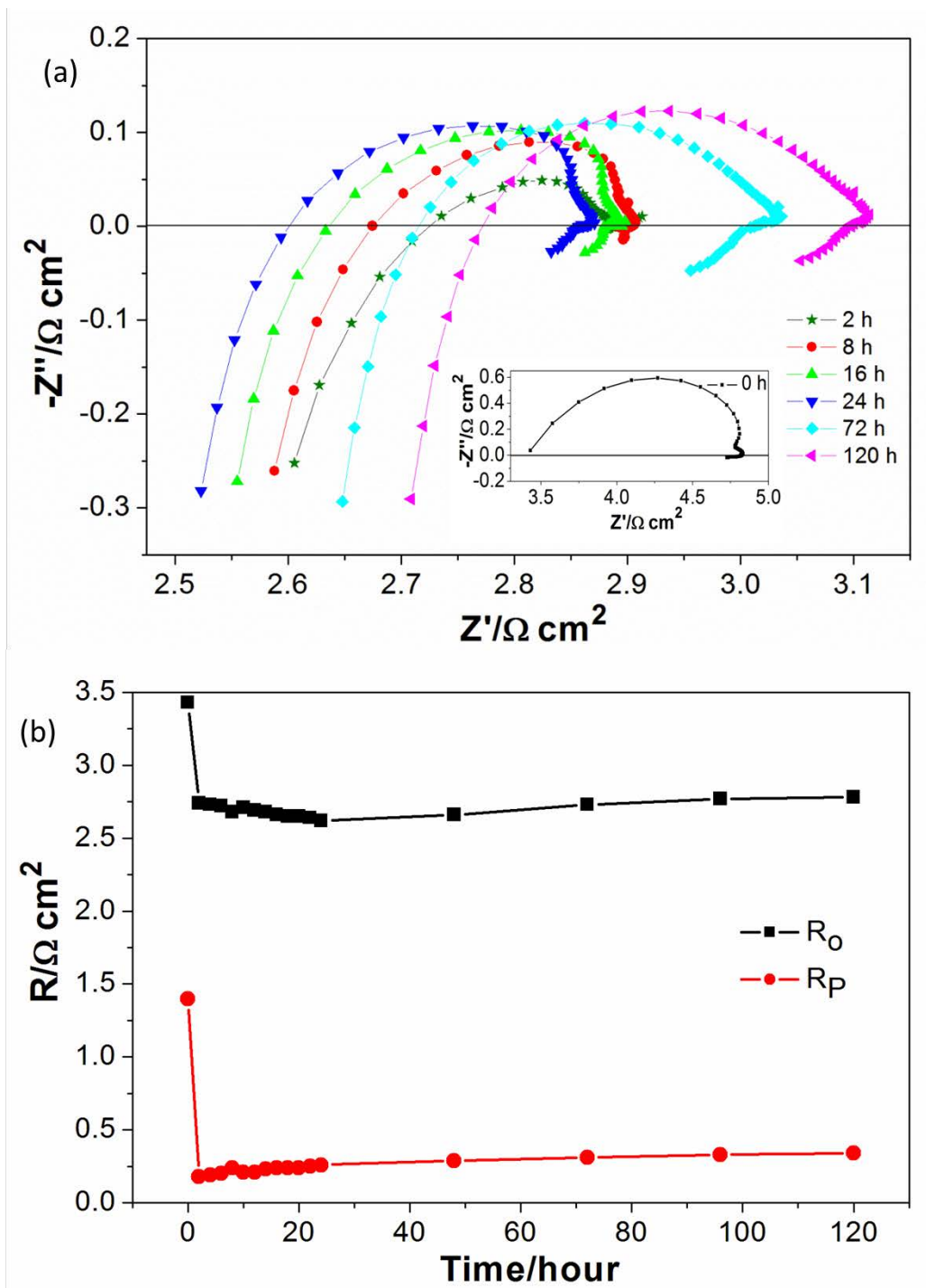


Fig. 3

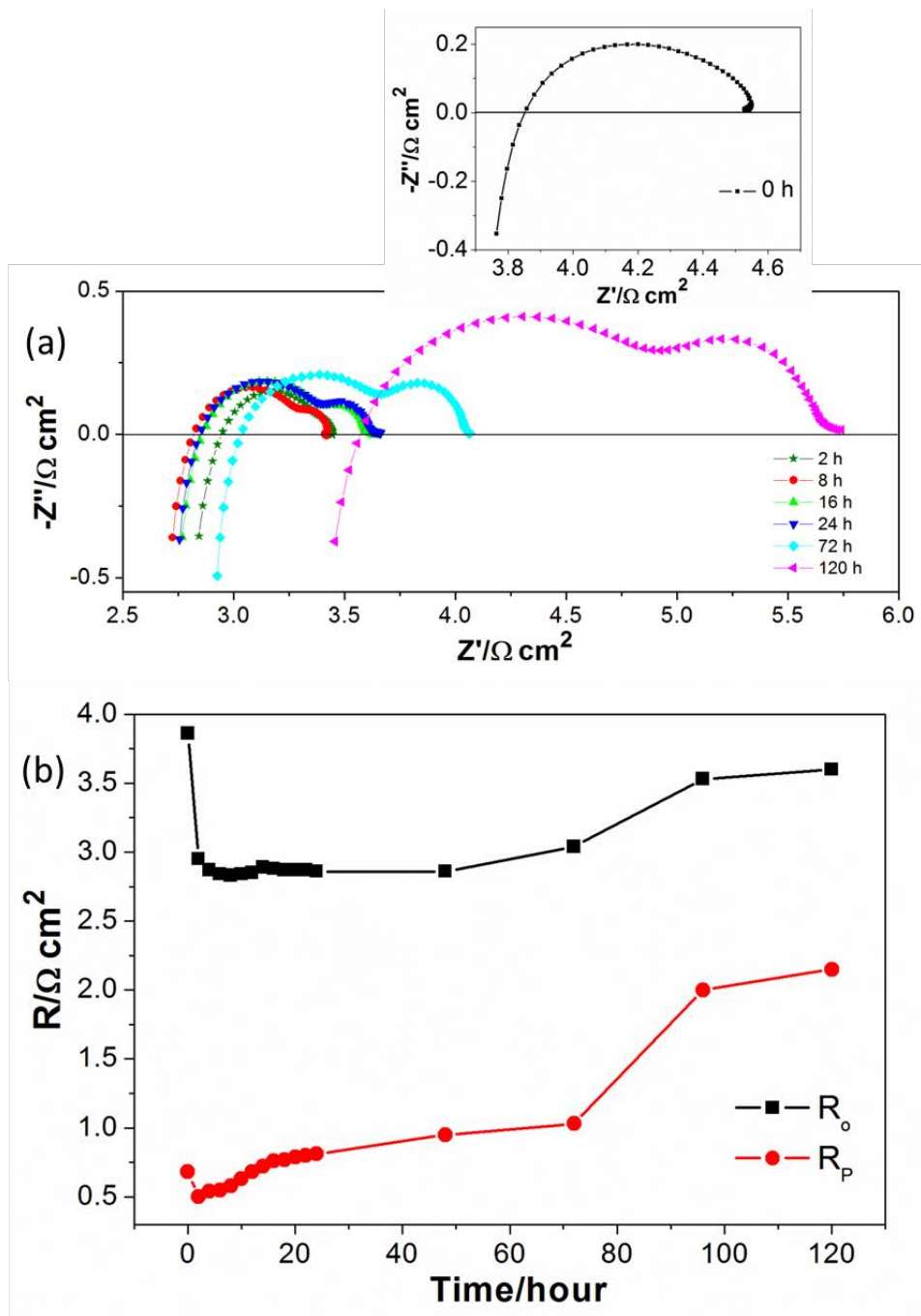
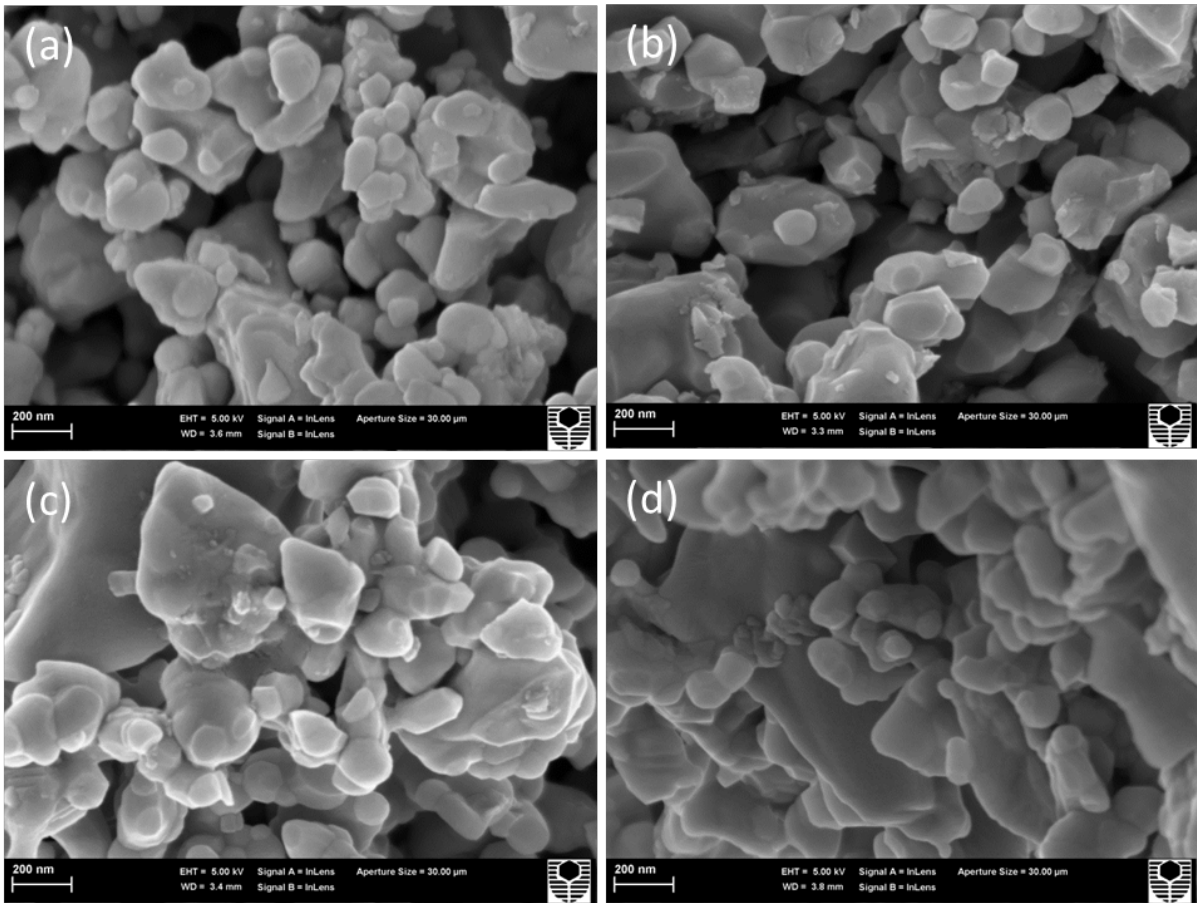
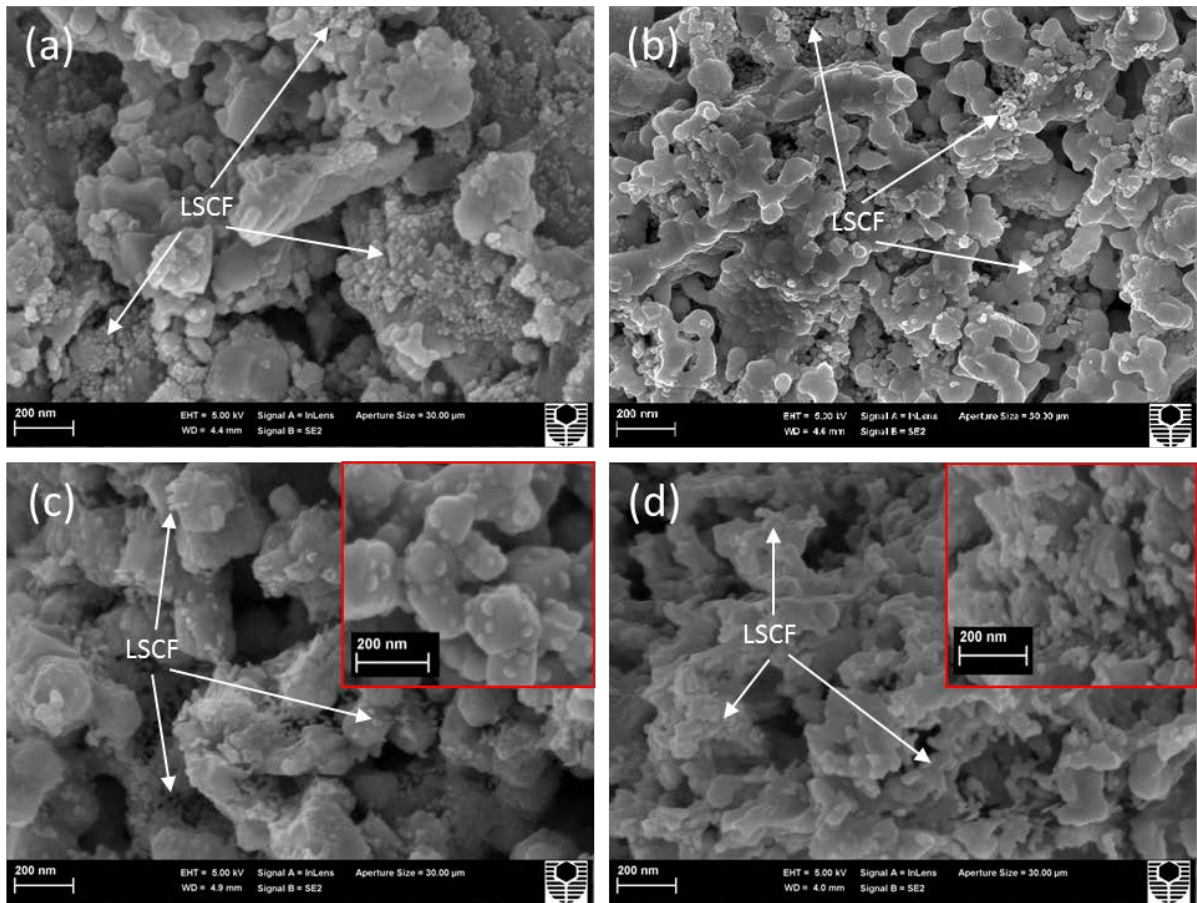


Fig. 4



**Fig. 5**



**Fig. 6**

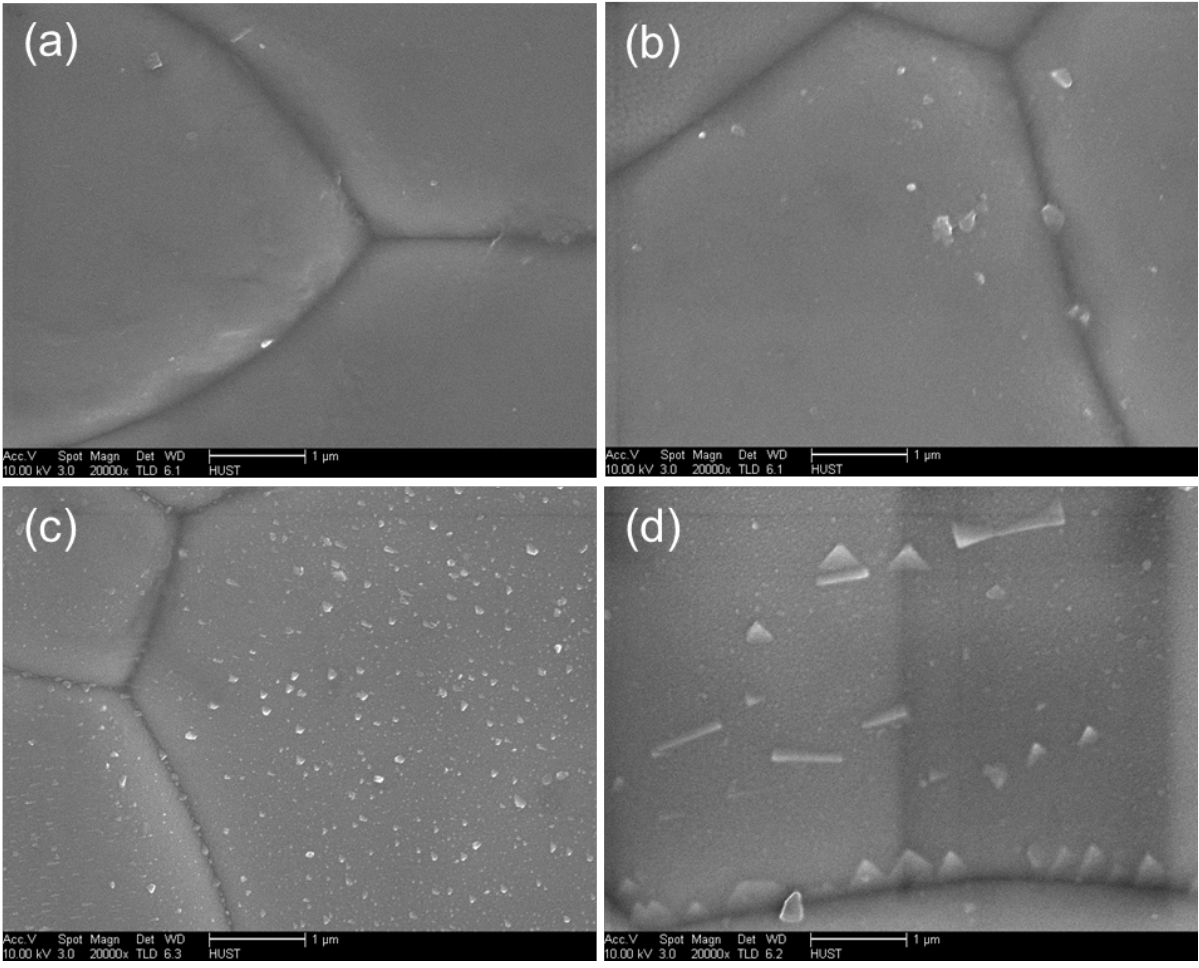


**Fig. 7**

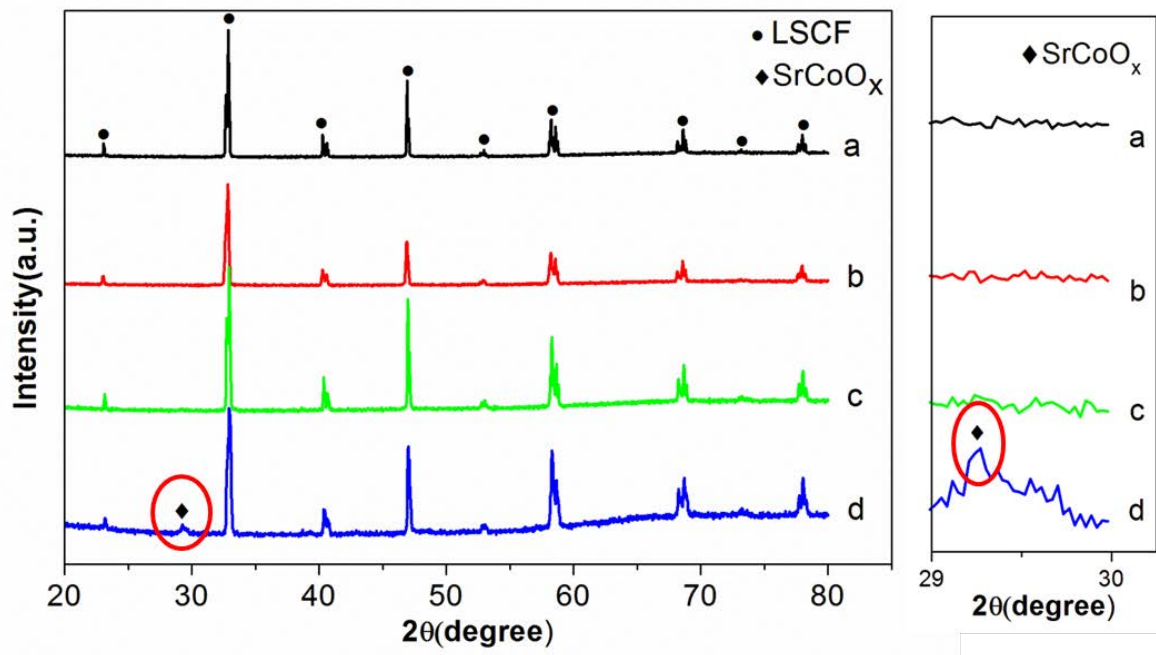
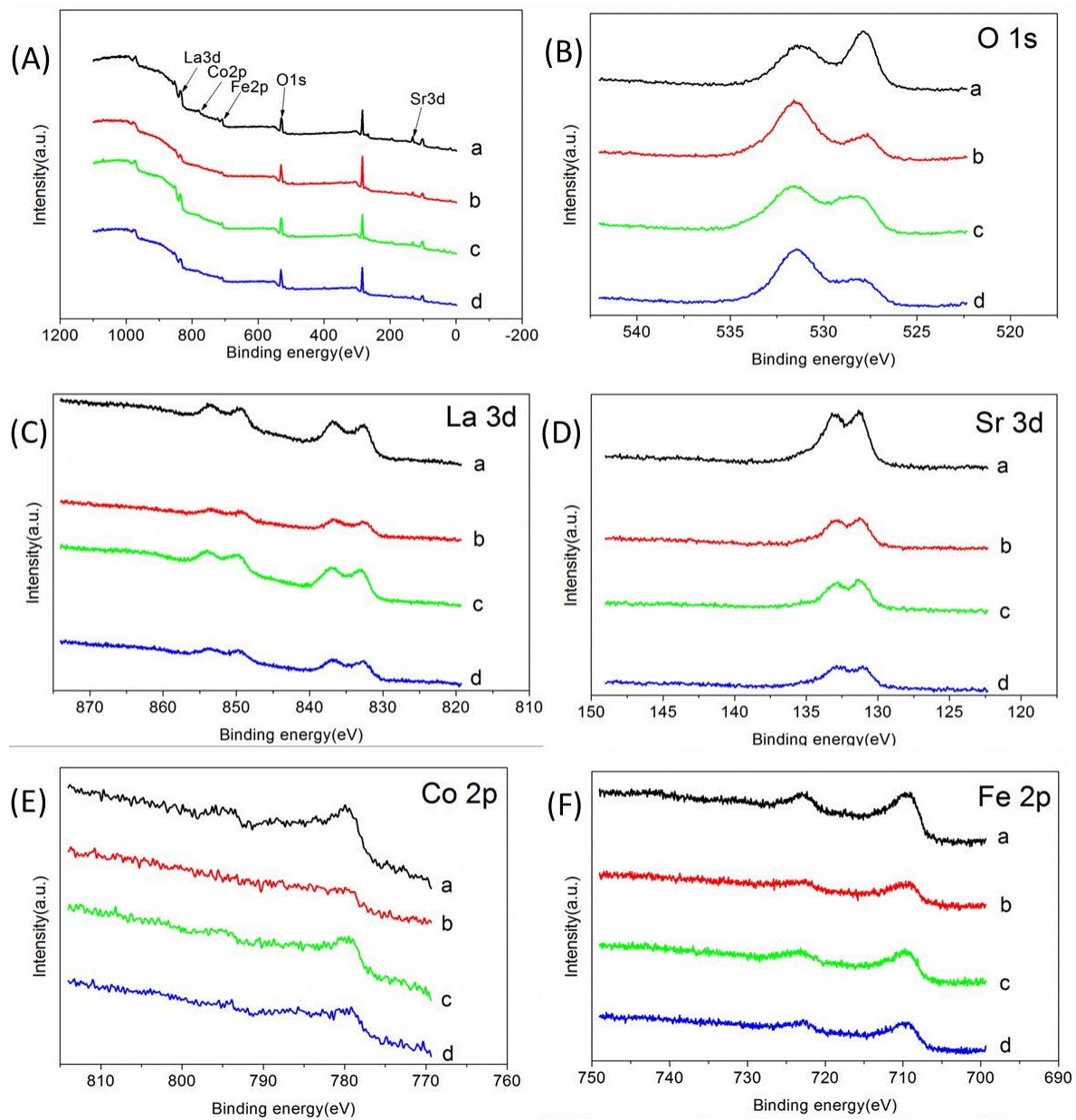


Fig. 8



**Fig. 9**